

# In situ kinetics study of the formation of organic nanoparticles by fluorescence lifetime imaging microscopy (FLIM) along a microfluidic device

Yuanyuan Liao<sup>1,2</sup> · Valérie Génot<sup>1</sup> · Jean-Frédéric Audibert<sup>1</sup> · Robert B. Pansu<sup>1</sup>

Received: 9 December 2015 / Accepted: 17 February 2016 / Published online: 19 March 2016  
© Springer-Verlag Berlin Heidelberg 2016

**Abstract** In this study, a three-dimensional hydrodynamic focusing microfluidic method is presented that allows full control of the nano-precipitation process of adamantyl mesityl BODIPY (4,4-difluoro-3,5-di-(adamantyl)-8-mesityl-4-bora-3a,4a-diaza-s-indacene) (Adambodipy). The precipitation is achieved by combining a central Adambodipy organic flow with a mixture of water and a cationic surfactant, creating a non-solvent precipitation method. The flow and mixing were simulated using COMSOL Multiphysics<sup>®</sup> 3.4. A good agreement between theory and experiment was obtained for the flow velocity, concentration fields and the subsequent precipitation kinetics. Fluorescence lifetime imaging was used to visualize the precipitation domains following the changes in fluorescence lifetime. The lifetime decreases from 6.1 ns for the molecules down to 0.9 ns for nanoparticles. A principal components analysis of the successive fluorescence decay curves showed that the process could be adequately modeled using three components, which can be attributed to monomers (single molecule), clusters (nuclei) and nanoparticles.

**Keywords** Fluorescent organic nanoparticles (FON) · 4,4-Difluoro-4-bora-3a · 4a-Diaza-s-indacene (BODIPY) · Computational fluid dynamics (CFD) · Hydrodynamic focusing · Precipitation

## Abbreviations

BODIPY	4,4-Difluoro-4-bora-3a, 4a-diaza-s-indacene
CTACl	Hexadecyltrimethylammonium chloride
DLS	Dynamic light scattering
E/EtOH	Ethanol
FLIM	Fluorescence lifetime imaging
FONs	Fluorescent organic nanoparticles
ID	Inner diameter of the channel
MEMS	Microelectromechanical systems
MFD	Micro-fluidic-device
NPs	Nanoparticles
OD	Outside diameter
PDMS	Polydimethylsiloxane
ROI	Region of interest
THF	Tetrahydrofuran

## List of symbols

$\phi$	Quantum yield
$\nabla$	Del operator
$\nabla c$	Concentration gradient
$\mu$	Viscosity
$\rho$	Fluid density
$a$	Particle size, radius
$a_0$	Diffusion length of exciton
$d_Q$	Density of quenching sites
$D_{ij}$	Maxwell–Stefan binary diffusion coefficient
$f$	Molar volume fraction of EtOH in the mixture
$J$	Jouyban–Acree factor
$k_F$	Fluorescence rate
$k_Q$	Quenching rate
$M$	Total average molar mass of the mixture (kg/mol)
$N$	Avogadro's number
$n_0$	Refractive index
$n(a)$	Number of quenching sites

✉ Yuanyuan Liao  
yuan-yuan.liao@ens-lyon.fr; yuanyuanliao@gmx.com

<sup>1</sup> Laboratoire PPSM, UMR 8531 du CNRS, ENS-Cachan, 61 av. Pdt Wilson, 94230 Cachan, France

<sup>2</sup> Present Address: UMR 5182 du CNRS, ENS-Lyon, 46 Allée d'Italie, 69364 Lyon Cedex 07, France

$P$	Pressure
$\Delta P$	Pressure drop
$Q_{(C,S)}$	Volumetric flow rate ( $C$ = center, $S$ = side)
$S$	Supersaturation
$U$	Local velocity of the fluid
$V$	Molar volume
$w$	Mass fraction
$W$	Water
$x_i$	Mole fraction of species $i$

## 1 Introduction

Fluorescent organic micro- and nanocrystals have numerous advantages as nanosensors due to their brightness and sensitivity (Meallet-Renault et al. 2006; Li et al. 2013). Their preparation has been reported using the reprecipitation method (Chung et al. 2006) and microwave irradiation (Baba et al. 2003). In recent years, controlled organization, shape and stabilization of organic nanoparticles (NPs) have attracted considerable research in pharmaceutical applications, special electronic components or used as pigment for imaging (Ofuji et al. 2005).

This 2D-hydrodynamic focusing microfluidic method demonstrates its ability to achieve rapid diffusion (Knight et al. 1998) capable of diffusive mixing time less than 10  $\mu$ s. This allows the progress of chemical reactions to be followed in the milliseconds immediately after initiating the mixing (Hessel and Lowe 2004). A 3D hydrodynamic focusing microfluidic setup was used to control the cross-sectional area and location of the focusing stream, as well as the supersaturation condition, by varying the flow rates and the concentrations of the surfactant and the sample. With supersaturation reached in a short time, generation of numerous nuclei was induced and the growth of nanocrystal was thus limited and controlled (Su et al. 2007; Génot et al. 2010).

Also, microfluidics has a great potential advantage for chemical analysis and synthesis by combining processes such as mixing, separation (Harrison et al. 1993), reaction and also detection in one single system (Hibara et al. 2003). It has been connected to several spectroscopic probes such as Fourier transform infrared (Kakuta et al. 2003a) and nuclear magnetic resonance (Kakuta et al. 2003b) spectroscopy in order to study the intermediate states in reactions. Combining a microfluidic device with fluorescence imaging technique functions as “labs-on-a-chip”, builds up a technology to follow the kinetics of a number of physical processes, such as concentration diffusion (Kamholz et al. 2001) and interface fluctuations (Hibara et al. 2003). The fluorescence time-resolved techniques could provide the appropriate lifetime information to map the molecule’s reactions with its surroundings, as the lifetime is sensitive to molecular assembly

(Teixeira et al. 2012), pH changes (Lin et al. 2003), diffusion (Roth et al. 2007), quenching (Boreham et al. 2011) and conformation changes (Calleja et al. 2003).

In this paper, microfluidic technology, including 3D hydrodynamic focusing and fluorescence lifetime imaging microscopy (FLIM), was used for a controlled formation of the organic NPs. The crystallization process was achieved by a reprecipitation method, and this process can be visualized and studied by time-resolved single-photon counting (Spitz et al. 2008). The potential application of this work also includes the design of microfluidic devices based on the fabrication of a Y-type (polydimethyl siloxane) PDMS/glass and glass/glass capillaries systems, and the simulation of the hydrodynamics and of the diffusion processes by the COMSOL Multiphysics® 3.4 (COMSOL, Inc. Burlington, MA) computational fluid dynamics (CFD) suite.

## 2 Materials and methods

### 2.1 Operation and design of the microfluidic system

The microfluidic systems to produce NPs are manufactured by photolithography of the mold (SU8 on silicon wafer), followed by curing of the PDMS elastomer and finally by O<sub>2</sub> plasma sealing on the glass substrate. The hydrodynamic focusing device was designed as shown on the flow pattern in Fig. 1. A capillary silica tube (from Polymicro, outside diameter (OD) = 150  $\mu$ m, inner diameter (ID) = 20  $\mu$ m) is inserted at the edge of the PDMS block and glued to fix it and avoid leakage. This capillary tube ensures the injection of the organic solution in the center of the squared PDMS main channel. It avoids interactions of the organic solvent, tetrahydrofuran (THF) and Adambodipy with the hydrophobic PDMS wall that may be swelled by the solvent or polluted by adsorption of the dye.

The solutions of Adambodipy were prepared in a mixture of THF with ethanol (EtOH), a so-called THF/EtOH

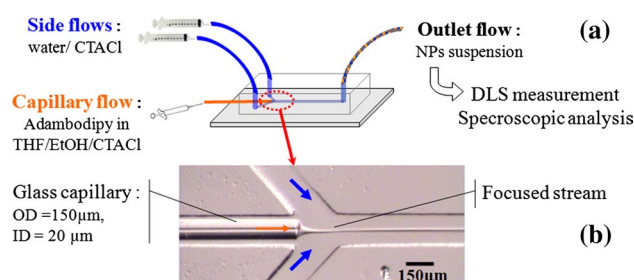


**Fig. 1** Microfluidic device. *a* Microchannel patterned in PDMS block, sealed to the glass substrate with the inserted capillary silica tube. The Y-type device connected for feeding and withdraws. *b* Details of the cross-junction area and of the laminar flow, focused stream of organic solution “squeezed” by the aqueous one

organic solvent [volume ratio THF/EtOH (v/v) = 3/7]. The concentrations of Adambodipy were 0.2 g L<sup>-1</sup>. A cationic surfactant hexadecyltrimethylammonium chloride (CTACl) was used as surfactant in this experiment and was added to both solutions at a concentration of 10<sup>-3</sup> mol L<sup>-1</sup>. The critical micelle concentration of this surfactant is around 1.3 × 10<sup>-3</sup> M. The side flow rate varied between 10–50 μL min<sup>-1</sup> and the capillary flow rate range between 0.5 and 3 μL min<sup>-1</sup>. We create a focused stream by flowing of the Adambodipy organic solution into a capillary tube in the middle of the aqueous solution flowing from the two inlet side channels. The three flows are all forced through the channel via two commercial syringe pumps (Harvard type PHD 2000 and Harvard Picoplus 11). For the further analysis, DLS and spectroscopic measurements, the volume required and collected at the outlet of the device is between 500 μL and 1 mL, which correspond to a run time between 10 and 40 min depending on the flow rates.

To perform the kinetics study, instead of a glass/PDMS microfluidic system, a new glass microchip was made to avoid the pollution of the PDMS by the spreading of fluorescent molecules so as to increase the signal-to-noise ratio of the fluorescence measurement. With a poly (ether ether ketone) (PEEK®) 7-port manifold (Upchurch Scientific®) as a connector, a small glass capillary (Polymicro, ID = 20 μm, OD = 90 μm) was inserted into a larger one (Polymicro, ID = 200 μm, OD = 350 μm) as shown in Fig. 2. A focused stream was created by flowing the organic solution of Adambodipy in THF/EtOH into the surrounding flow of water, both containing CTACl, using the same syringe pumps to force the flow by syringes through the microchannel.

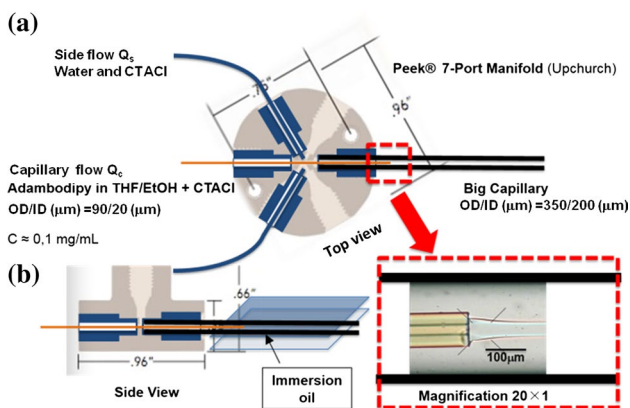


**Fig. 2** a Schematic representation of 3D-hydrodynamic microfluidic device from the top and the side b and the details of the cross-junction area of the flow under microscope in (c)

## 2.2 Dynamic light scattering (DLS)

The Adambodipy NPs suspension was analyzed by a dynamic light scattering analyzer (DL135 Particle Size Analyzer, Cordouan Technologies) equipped with a 15 mW diode laser, operating at 650 nm. An original design of the sample cell is proposed to enhance the DLS instrument with back-scattered light detection at an angle of 135° and the capability to control the sample thickness. This apparatus offers a configuration which allows analyzing as little as a 50 μL sample volume. The main limitation concerns dilute suspensions (2 × 10<sup>-6</sup> g mL<sup>-1</sup>), when the signal is difficult to discriminate from the noise.

## 2.3 Fluorescence lifetime imaging microscopy (FLIM)

Fluorescence lifetime imaging microscopy (FLIM) with a space- and time-resolved single-photon counting device is used to visualize the precipitation process in this experiment. Indeed, fluorescence is a sensitive technique and its spectrum and lifetime are sensitive to molecular organization and interactions (Spitz et al. 2008).

We have implemented fluorescence lifetime imaging, because it is even more sensitive to molecular interactions.

The fluorescence generated from the sample is guided to a space- and time-resolved single-photon counting photomultiplier (QA) from Europhoton GmbH (Berlin, <http://www.europhoton.de/>). For each photon, its position and arrival time is measured and stored. From these data files, both intensity and lifetime images can be calculated (Badre et al. 2006).

The experimental device is shown in Fig. 3. The pulsed laser source is an Ytterbium TPulse200 from Amplitude Systèmes (Pessac France). It is injected into the microscope (Nikon 2000 TE) through the epi-illumination port of an inverted microscope (Nikon S-Fluor, 40, 0.90 NA).

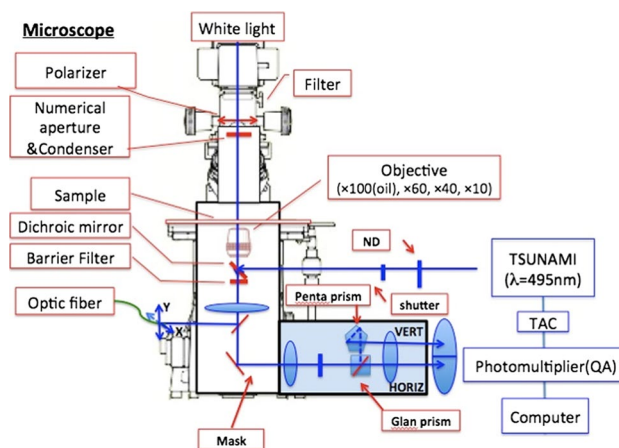


**Fig. 3** Time-resolved single-photon counting device

In addition to the QA device, the spectra (absorption and fluorescence) are collected by means of a fiber-coupled spectrometer (Ocean Optics, Inc., ZD2000, fiber diameter = 600  $\mu\text{m}$ ) (Spitz et al. 2008).

The FLIM measurement is taken with a multi-channel plate photomultiplier working in the single-photon counting mode.

## 2.4 COMSOL simulation

The simulation of the flow diffusion processes to predict the concentrations and velocity field in the 3D hydrodynamic microfluidic device was performed using COMSOL. The geometry was built with the same dimension as the setup used in the kinetics experiment. Thanks to the cylindrical geometry of the glass device, we applied the axial-symmetry calculation mode. The simulation temperature was set to 298 K.

### Step 1: simulation of the velocity field

Since the flow in this research is considered as a continuum, the Navier–Stokes equations are applicable. Also because the flow of water is being modeled, mixed with THF/EtOH in microfluidics, where the flow velocities are much smaller than the velocity of pressure waves in the liquid, incompressibility and Newtonian fluid assumptions may be used here.

The steady-state “Incompressible Navier–Stokes” (MEMS Module) model for a laminar flow and a Stokes regime was invoked. The following equation was first used to solve the momentum conservation and the velocity profile for the fluid flow in the channel, considering two incompressible solutions without diffusion:

$$\left( \rho \frac{\partial u}{\partial t} - \nabla \cdot [(-p)I + \mu(\nabla u + (\nabla u)^T)] + \rho u \cdot \nabla u \right) = F \quad (1)$$

$$-\nabla u = 0 \quad (2)$$

where  $\rho$  ( $\text{kg m}^{-3}$ ) is the fluid density,  $u$  is the flow velocity vector,  $p$  is the fluid pressure (Pa),  $I$  is the unit diagonal matrix,  $\mu$  is the fluid’s dynamic viscosity (Pa s) and  $F$  (N) is a bulk force affecting the fluid. In our case,  $\frac{\partial u}{\partial t}$  and  $F$  are equal to 0, and the inertial term is neglected. In this model, the properties of both the organic and aqueous solutions are, respectively, considered at ambient temperature:  $\rho_E = 789 \text{ kg m}^{-3}$ ,  $\mu_E = 1.2 \times 10^{-3} \text{ Pa s}$  and  $\rho_W = 1000 \text{ kg m}^{-3}$ ,  $\mu_W = 10^{-3} \text{ Pa s}$ . Then we obtained the velocity profile based on the plot of microfluidic device.

We first mesh with the parameters in Table 1. We fixed the initial velocity at a value of  $0.04246 \text{ m s}^{-1}$  for side flow and  $0.01810 \text{ m s}^{-1}$  for center flow, according to the flow rate of 13.6 and  $0.8 \mu\text{L min}^{-1}$ . The other boundary conditions were set as “no slip” along the wall and “atmospheric pressure” at the outlet. From the given surface of the

**Table 1** Mesh statistics used for the calculation

Number of degrees of freedom	106,443
Number of mesh points	6341
Number of elements	12,344
Triangular	12,344
Quadrilateral	0
Number of boundary elements	404
Number of vertex elements	9
Minimum element quality	0.6738
Element area ratio	0.1813

channel, we solve the Incompressible Navier–Stokes model (MEMS Module) with stationary solver (cf. Table 2) for velocity distribution over the channel. The following calculations were done with initial value expression evaluated using the current solution.

### Step 2: interdiffusion simulation of the two solutions

Based on the results of the initial calculation of the velocity profile, the “Maxwell–Stefan Diffusion and Convection” (Chemical Engineering Module) model was then applied here to determine the mixing of organic and aqueous solutions via counter diffusion along the laminar flow.

$$\nabla \cdot \left[ -\rho w_i \sum_{j=1}^N D_{ij} \left\{ \frac{M}{M_j} \left( \nabla w_j + w_j \frac{\nabla M}{M} \right) + (x_j - w_j) \frac{\nabla p}{p} \right\} + w_i \rho \bar{u} \right] = 0 \quad (3)$$

$$x_j = \frac{w_j}{M_j} \cdot M \quad (4)$$

$$\sum_{i=1}^n w_i = 1 \quad (5)$$

where  $M$  denotes the total average molar mass of the mixture ( $\text{kg mol}^{-1}$ ),  $M_j$  gives the molar mass of species  $j$  ( $\text{kg mol}^{-1}$ ) and  $w_j$  is the mass fraction of species  $j$ .

In addition, with the “Maxwell–Stefan Diffusion and Convection” module in binary system, the self-diffusion coefficient data used for water and ethanol were taken from the literature.  $D_W = 2.299 \times 10^{-9} \text{ m}^2 \text{ s}^{-1}$  (Holz et al. 2000),  $D_E = 1.07 \times 10^{-9} \text{ m}^2 \text{ s}^{-1}$  (Guevara-Carrion et al. 2008). Then the Maxwell–Stefan diffusion coefficient  $D_{W-E}$  was estimated from the self-diffusion coefficients of the two components  $D_W$  and  $D_E$  in the binary mixture (Darken 1948)

$$D_{W-E} = x_W \cdot D_E + x_E \cdot D_W \quad (6)$$

### Step 3: rerun the steady-state “Incompressible Navier–Stokes” calculation

The “Incompressible Navier–Stokes” calculation was solved again at a higher level of refinement with the value

**Table 2** Solver parameters

Analysis	Stationary
Linear system solver	Direct UMFPACK
Matrix symmetry	Automatic
Linearity	Automatic
Relative tolerance	10 <sup>-7</sup>
Maximum no. of iterations	40

of mutual diffusivity, density and local viscosity coming from the last step.

The solutions taken into consideration were, respectively, ethanol and water. Then, the value of mutual diffusivity, density and viscosity along the flow of this water–ethanol binary system was calculated with the input scalar expressions (Eqs. 3–5) with the mass fraction profile results.

Considering the change in density and viscosity of the fluids since they mixed during the flowing, the Jouyban–Acree estimation was used in the simulation. The following relation was used by the author to fit the density and the viscosity of the binary mixture of water and ethanol (Khatat et al. 2012):

$$\ln \rho_{m,T} = x_W \cdot \ln \rho_{W,T} + x_E \cdot \ln \rho_{E,T} - 30.808 \left[ \frac{x_W \cdot x_E}{T} \right] - 18.274 \left[ \frac{x_W \cdot x_E \cdot (x_W - x_E)}{T} \right] + 13.890 \left[ \frac{x_W \cdot x_E \cdot (x_W - x_E)^2}{T} \right] \tag{7}$$

$$\ln \eta_{m,T} = x_W \cdot \ln \eta_{W,T} + x_E \cdot \ln \eta_{E,T} - 724.652 \left[ \frac{x_W \cdot x_E}{T} \right] + 729.357 \left[ \frac{x_W \cdot x_E \cdot (x_W - x_E)}{T} \right] + 976.050 \left[ \frac{x_W \cdot x_E \cdot (x_W - x_E)^2}{T} \right] \tag{8}$$

with  $T$  (K) the temperature and  $W$ ,  $E$  and  $m$  subscripts standing for water, ethanol and their mixtures, respectively. The  $R^2$  values for Eqs. (7–8) are 0.986 and 0.945, respectively.

*Step 4: the “Convection and Diffusion” module*

Subsequently, the velocity field obtained from the “Incompressible Navier–Stokes” simulation was implemented for the calculation of the concentration distribution of the dye using the “Convection and Diffusion” module. The diffusion of Adambodipy species in the water–ethanol system under microfluidic flow conditions was then solved according to the convection–diffusion equation:

$$-\nabla \cdot (-D\nabla c + cu) = 0 \tag{9}$$

*Step 5: supersaturation profile calculation*

From these calculations, profiles of the density, viscosity, mutual diffusivity, concentration of Adambodipy and mass fraction of water and ethanol at local positions along the flow are obtained. Combining these results with the input scalar expression for solubility of the Adambodipy in the binary system (Eq. 11) and the supersaturation expression (Eq. 10), the “Maxwell–Stefan Diffusion and Convection” module was rerun to obtain the supersaturation profile (Fig. 10).

The geometry and the dimensions are those of the experimental device of the glass microchip shown in Fig. 2. Again, due to the device symmetry, a 2D-axisymmetric model was chosen here.

**2.5 Supersaturation property**

The supersaturation  $S$  was defined as the ratio of actual concentration of Adambodipy to the solubility  $C_{eq}$ . This is the barrier that determines the kinetics of nucleation (Abraham 1974; Nielsen 1964)

$$S = \frac{C_{Adambodipy}}{C_{eq}} \tag{10}$$

According to the supersaturation equations, the  $C_{Adambodipy}$  profile could be calculated from the former COMSOL simulation using the “Convection and Diffusion” module; however, in order to determine the value of  $C_{eq}$ , we need to introduce another predictive model.

As we are using a binary water–ethanol mixture in the simulation, the mixture fluids have a different density and viscosity in the inlet channel, side channel and outlet channel since they mixed during the flowing. A suitable model to predict the solubility curves of dyes in a binary water–ethanol mixture was developed by Jouyban (Jouyban and Acree 2006) and has the following form:

$$\log S_{mix} = \log S_E + (1 - f) \log S_W + J \tag{11}$$

where  $S_{mix}$ ,  $S_E$  and  $S_W$  are the solute solubility at temperature  $T$  in the mixed solvent, neat co-solvent and water, respectively;  $f$  is the volume fraction of the (co-solvent) EtOH in the mixture, where  $V_E$  and  $V_W$  are the molar volume of EtOH and water:

$$f = \frac{V_E}{V_W + V_E} \tag{12}$$

The Jouyban–Acree factor ( $J$ ) that takes into account the non-ideality of the mixing is estimated by:

$$J = f(1 - f) \left[ \frac{724.21}{T} + \frac{485.17(f - (1 - f))}{T} + \frac{194.41(f - (1 - f))^2}{T} \right] \tag{13}$$

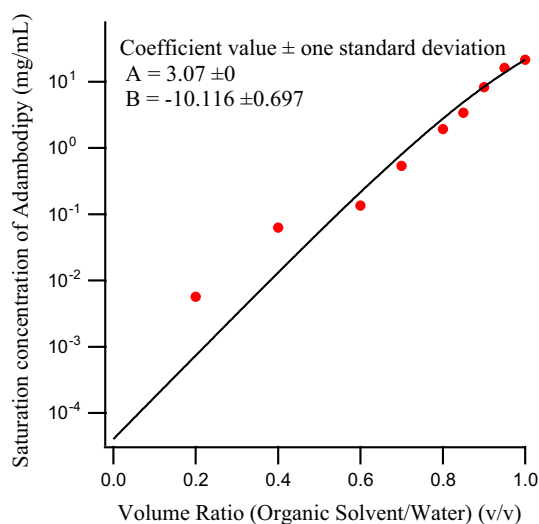


**Fig. 4** Experimental solubility points for Adambodipy in the mixture of organic solvent with water [the organic solvent being THF/EtOH ( $v/v = 3/7$ ), fitted to the Jouyban–Acree model logarithmically

An experimental solubility curve for Adambodipy in the mixture of THF/EtOH( $v/v = 3/7$ ) with water has been made.

We have adjusted the data according to the Jouyban–Acree model through a logarithmic fit with  $T = 298$  K and the expression would be:

$$G(f) = \exp(Af + B(1-f) + f(1-f)) * \left[ \frac{724.21}{298} + \frac{485.17(f - (1-f))}{298} + \frac{194.41(f - (1-f))^2}{298} \right] \quad (14)$$

The result of the fit is shown in Fig. 4. We obtained for the adjustable parameters values of:  $A = \ln S_E$ ,  $B = \ln S_W$ , while  $A = 3.07$ ,  $B = -10.116$  according to the concentration of Adambodipy when the percentage of water equals 0. Using this framework, the saturation solubility  $C_{eq}$  of Adambodipy in a known composition of water–EtOH solvent can be calculated, where in this experiment, the mass composition of the water–ethanol mixture could be simulated with COMSOL using the “Maxwell–Stefan Diffusion and Convection” module through a simple conversion from the mass fraction (as used by this module) to the volume fraction (as used here).

### 3 Results and discussion

#### 3.1 Nanoparticles analyses

The concentration of Adambodipy in the organic solution was fixed to 0.3 mM. The flow rates  $Q_s/Q_c$  were maintained below 40 to avoid particles remaining undetected in DLS and above 13.3 to avoid the formation of

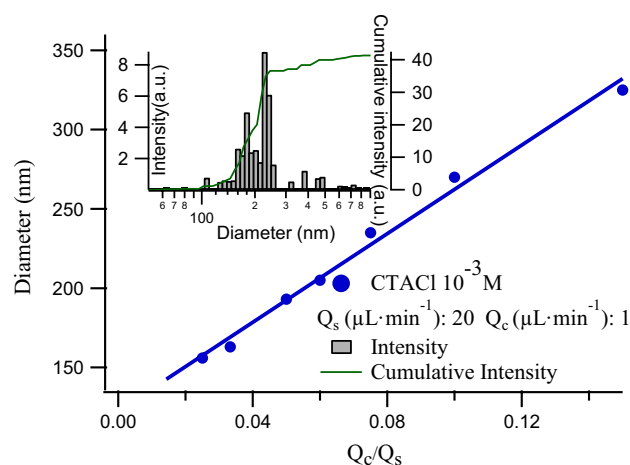


**Fig. 5** Demonstrating how DLS intensity and distribution varies in response to the condition of different flow rate ratio by MFD. Size distributions of Adambodipy NPs produced at flow rate  $Q_s = 20 \mu\text{L min}^{-1}$ ,  $Q_c = 1 \mu\text{L min}^{-1}$ . *b* Diameters of NPs suspension as the function of  $Q_c/Q_s$ . Those NPs suspension samples are collected with concentration of CTACl =  $10^{-3}$  M,  $C_{\text{Adambodipy}} = 0.2 \text{ mg mL}^{-1}$  in THF/EtOH ( $v/v = 3/7$ ) as organic solution

4,4-difluoro-4-bora-3a, 4a-diaza-s-indacene (BODIPY) derivative crystalline precipitate on the nozzle.

Figure 5a shows that with the use of the MFD, the NPs of Adambodipy are produced and the size distribution can be measured by DLS, DLS being a powerful method to determine small changes in particle size.

The radii of the NPs can be plotted as a function of  $Q_c/Q_s$  in Fig. 5b, and the relationship is approximately linear. As shown, the size distribution of NPs can be tuned by varying the flow rate ratio. As  $Q_s/Q_c$  increases from 13.3 to 40, the NPs become smaller, from 240 to 160 nm. This effect can be related to the hydrodynamics coupled with the diffusion in the microdevice. The supersaturation governed the kinetics of nucleation and growth mechanisms and finally the size of the NPs. As the flow rate ratio  $Q_s/Q_c$  increases, the width of the focused stream decreases, changing the kinetics to reach the supersaturation in the focused stream. In addition, the DLS intensity decreased, due to the lower concentration of the organic solution of Adambodipy. By re-examining the DLS intensity of those samples after several days (from 1 to 4 days), we found that the NPs suspension samples produced here are quite stable in the presence of surfactant. These experiments and the observed trends in particle size are also reproducible.

To investigate the hydrodynamic focusing under stable flow within the device, we monitored the flow rate ratio from 30 to 45 with a low and identical total flow rate. We chose a fixed residence time of 8 ms in order to fix the contribution of diffusion of Adambodipy. A residence

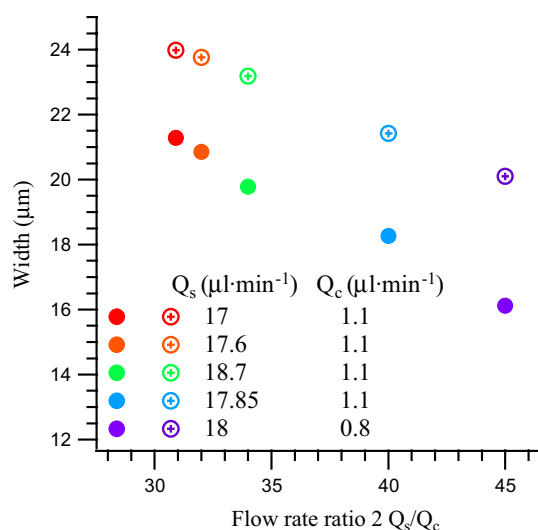


**Fig. 6** Widths of the focused stream at the position corresponding to a residence time of 8 ms as a function of the flow rates ratios, experimental (filled circles) and theoretical values (circles with + symbol)

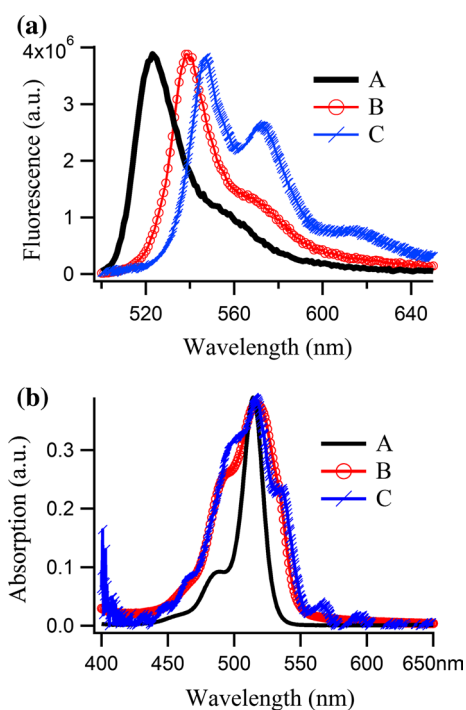


**Fig. 7** **a** Fluorescence spectra for sample A were from a sample of Adambodipy monomer in THF/EtOH (v/v) = 3/7 with CTACl ( $10^{-3}$  M), and B was produced with MFD, both excited at 495 nm, with a maximum at 539 and 570 nm, respectively, using identical experimental parameters. The fluorescence spectrum C of the single crystal was recorded, excited at 343 nm with main band at 547 and 573 nm. Then, the absorption spectra for the same sample A, B and C are compared in **(b)**

time of 8 ms corresponds to a position far ( $50 \mu\text{m}$ ) from the bulb, the transition flow that is present close to the nozzle. Then the width for each flow rate ratio can be determined at this position, as the full width at half maximum (FWHM) of the cross section of the fluorescence on each image.

These widths were also determined from numerical simulations using COMSOL software with identical geometry (small capillary OD =  $45 \mu\text{m}$  inserted into a big capillary channel ID =  $100 \mu\text{m}$ ) and identical parameters for each flow. One example is given in the figure below the  $x$ -axis at position 0 on Fig. 11. The widths correspond to the FWHM of the concentration profile at the same position when  $\tau = 8$  ms. The hydrodynamic focusing was simulated including the diffusion of Adambodipy, and its diffusion coefficient was calculated from the Stokes–Einstein equation ( $4.23 \times 10^{-10} \text{ m}^2 \text{ s}^{-1}$ ).

The suspensions of Adambodipy NPs were also analyzed by absorption and fluorescence spectroscopy. For all the samples obtained at different flow rates ratios, the spectra are identical except in intensity as mentioned before for DLS measurements (Fig. 6).

Typical fluorescence and absorption spectra obtained for Adambodipy in solution and in solid states suspensions (NPs and microcrystal) are shown in Fig. 7.

The spectra can be compared with the calculated spectra of the amorphous and crystalline phases (computed from the X-ray diffraction spectra) (Liao et al. 2013).

Figure 7b shows normalized absorption spectra for molecules in solution (A), for NP suspensions produced by MFD (B) and the microabsorption spectrum of an Adambodipy single crystal (C). They exhibit absorption maxima ( $\lambda_{\text{max}}$ ) at 514 nm for the molecules, and 517 nm for the sample B and single crystal sample. In the microcrystal, the absorbance peaks are leveled off by a measurement artifact (light leaks around the crystal and interference phenomena are observed between the two crystal faces). The shoulder at 540 nm is characteristic of the crystalline state and is not seen in sample B from MFD. The difference of the absorption spectra between sample B and the microcrystal suggests that samples produced by MFD are amorphous.

In the fluorescence spectrum obtained for the microcrystal (curve C, Fig. 7a) produced by a slow crystallization (Liao et al. 2013), there is a red shift (24 nm) compared to the main band at 523 nm for the Adambodipy in solution. The band at 547 nm can be attributed to the crystalline structure of the Adambodipy. The band at 573 nm is characteristic of the crystal, and we know from polarization experiments that it is the superposition of the vibrational structure and a trapped exciton.

The sample B prepared by MFD exhibits a main fluorescence band at 539 nm and a shoulder around 570 nm. These values correspond to the one calculated on a simulated amorphous phase. This is in agreement with the fact that the MFD preparation methods can be considered to be a fast precipitation process.

### 3.2 Kinetic study of the precipitation process

The Adambodipy in the solid state has a shorter fluorescence lifetime and a lower quantum yield (0.9 ns and  $\Phi = 0.15$ ) compared to that of the molecule in the organic solution (these values being 6.1 ns and  $\Phi = 0.48$ , respectively). The decrease in the fluorescence lifetime is due to the depletion of monomer and the precipitation process. The decrease in the quantum yield during the precipitation process was compensated by the increase in both the acquisition time and the laser power.

A significant feature is that the width of the focused stream containing the dyes does not increase along the flow. Indeed, the diffusion coefficient of the particle is roughly inversely proportional to particle size according to the Einstein–Stokes theory (Kuhn and Waldeck 2009). Therefore, the diffusion coefficient of the particles will decrease during the NP growth process and prevent the migration across the channel.

Figure 8 shows that at position  $d = 0$  mm, the lifetime of the focused stream looks homogeneous and identical to the monomer solution flowing in and out of the capillary. The corresponding lifetime is in accordance with the lifetime of 6.1 ns measured in the *cuvette*. For the next image at position  $d = 1$  mm, the heterogeneity appears in the diffusion areas between the organic and the aqueous solutions, where the precipitation process starts.

For each image, the mean fluorescence decay along the channel is recorded. Those decays are normalized to  $10^4$  photon counts (cts.) and gathered in Fig. 9a. According to the figure, the average lifetime decreases along the

focusing flow. This can be related to the mixing of water with the EtOH/THF mixture, which reduces the solubility of Adambodipy and induces its precipitation.

Two regions of interest (ROIs) are shown in Fig. 8 at the interface (ROI1) and in the middle of the flow (ROI2), respectively. At each position along the flow, the fluorescence decays are collected in ROI 1 and ROI 2 separately. All those decays exhibit the same evolution with a continuous decrease in the fluorescence lifetime that can be related to a continuous consumption of Adambodipy molecules from solution to particles.

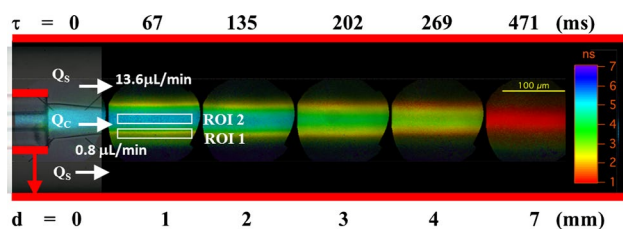
A principal component analysis of the data demonstrates that three decays are sufficient to interpret the data in a physically insightful way. The first one is the fluorescence decay of the monomer; the second one is the fluorescence decay of the nanoparticle. A third contribution arbitrarily set to an intermediate decay associated with position  $d = 3$  mm (as in Fig. 8) allows us to describe all the decays. This third compound associated with intermediate contribution is neither the monomer fluorescence nor the NP fluorescence. It is attributed to the presence of nuclei or clusters, i.e., the assembly of a few molecules with subcritical size. Their intermediate fluorescence lifetime is easily rationalized, since lifetime can be a function of aggregate size. Indeed the excited state (exciton) that is produced by the absorbed photon will diffuse in the NPs and the bigger the NPs are, the higher the number of quenchers is in the NPs that induces the decrease in the lifetime. When the particle becomes large compared to the diffusion length of the excitation, the quenching should reach a plateau.

Figure 9b shows the distribution of the three contributions along the channel at the interface (ROI 1) and in the middle of the flow (ROI 2). The evolution of the contribution is similar with a delay of 135 ms ( $d = 2$  mm) for the consumption of the monomer and a plateau of the intermediate contribution in the ROI 1, i.e., for the diffusion area at the edge of the focused stream.

At the interface, there is no more monomer after 70 ms, and the intermediate at the interface remains the dominant species up to 270 ms. Indeed monomers can diffuse from the center flow. The new subcritical intermediates are formed from the monomers, faster than they are consumed by aggregation.

In the middle of the focus stream, the monomer concentration decreases slowly over the three first millimeters (i.e., in the first 150 ms); then, it drops below 10 % of its initial value at 3.3 mm. From 3 mm to 4 mm (200 to 270 ms), the intermediate species dominate. In both ROIs, they are transformed into stable NPs at 7 mm (corresponding to 470 ms).

This transformation occurs at a point where there is no more monomer available. Thus, the growth of NPs still proceeds after monomer depletion. In this last phase, species



**Fig. 8** Representative fluorescence lifetime data from 3D-hydrodynamic focusing microfluidic system. The glass microchip shown in Fig. 2 was used here with the central flow of Adambodipy organic solution at the concentration of 0.08 mM,  $Q_c = 0.8 \mu\text{L min}^{-1}$ , sheathed by side flow of water,  $Q_s = 13.6 \mu\text{L min}^{-1}$ . Fluorescence lifetime images were taken at every millimeter along the channel



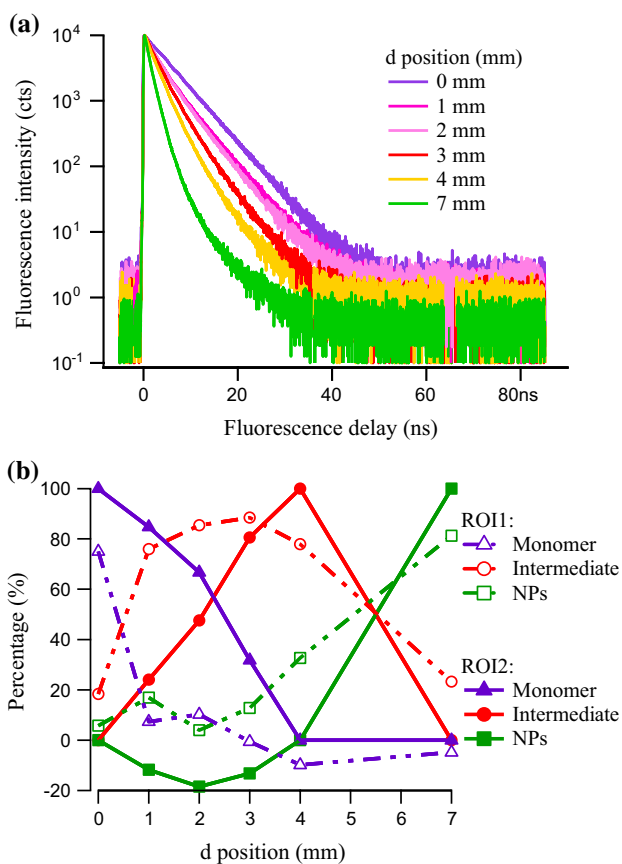


**Fig. 9** **a** Normalized mean fluorescence decays according to the FLIM images along the flow at different positions, **b** distribution of the three contributions describing the decays along the channel in the ROI 1 at the interface (*dashed lines*) and in ROI 2 in the middle of flow (*plain lines*). Each color (*marker*) corresponds to a contribution: purple (*triangle*) for the long decay (*monomer*)—red (*circle*) for intermediate decay—green (*square*) for fast decay (NPs) (color figure online)

of subcritical size continue to coagulate until essentially all particles reached a critical size.

As long as the NP size is smaller than the diffusion length of the exciton, the number of quenchers that are able to kill the fluorescence of the exciton will increase with the volume of the nanoparticle. The fluorescence decays exponentially:

$$I^*(t) = I^*(0) \exp [-(k_F + n(a)k_Q)t] \tag{15}$$

where  $k_F$  is the fluorescence rate,  $k_Q$  is the quenching rate,  $n(a)$  is the number of quenching sites in a particle of radius  $a$ .  $n(a) = d_Q \left(\frac{a}{a_0}\right)^3$ , where  $a_0$  is the diffusion length of the exciton and  $d_Q$  is the density of quenching sites.

As in theory that predicts that the nucleation and crystallization rates depend mainly on the degree of supersaturation, we may suggest that the concentration reaches the minimum saturation required to generate a critical free energy for nucleation. The COMSOL simulation will help to estimate this critical supersaturation value.

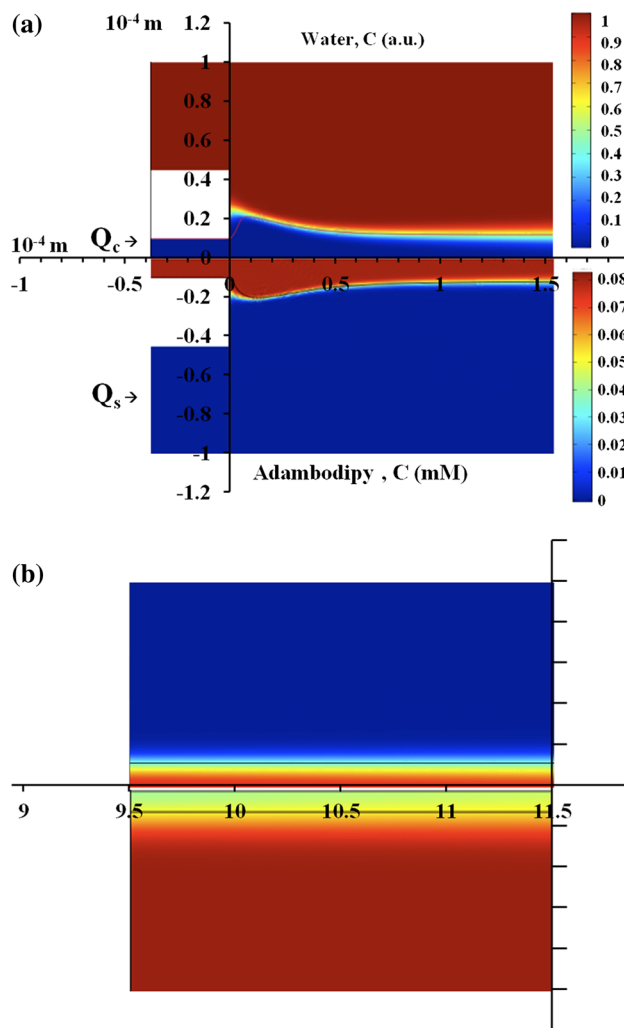


**Fig. 10** 2D-axisymmetric geometry of the glass microfluidic device and COMSOL simulations of diffusion in hydrodynamic focusing flow,  $Q_c = 0.8 \mu\text{L min}^{-1}$  and  $Q_s = 13.6 \mu\text{L min}^{-1}$ ,  $C_{\text{Adambodipy}} = 0.08 \text{ mM}$ . Concentration distributions of water (above the  $x$ -axis) and of Adambodipy (below  $x$ -axis) along the  $200 \mu\text{m}$  of the channel at position 0 (**a**) and at position 1 mm (**b**). The *streamline* indicates the interface between the two solutions (*color scales* define the value with the same unit as the main component) (color figure online)

From the former DLS experiment, the hydrodynamic focusing determines the quality of NP formation. The precipitation process is governed by interdiffusion of water and Adambodipy along the channel. The diffusion of water in the organic solution is much faster with a diffusion coefficient equal to  $1.6 \times 10^{-9} \text{ m}^2 \text{ s}^{-3}$ , as shown by comparison of top and bottom simulations in Fig. 10. In a first approximation, we can neglect the diffusion of Adambodipy. The simulation of water diffusion at 1 mm (Fig. 10b) indicates that the water has reached the middle of the focused stream. Nevertheless, the percentage of the water is below 65 % at  $r < 10 \mu\text{m}$ , whereas for an Adambodipy concentration of 0.08 mM, this water content is expected to start the

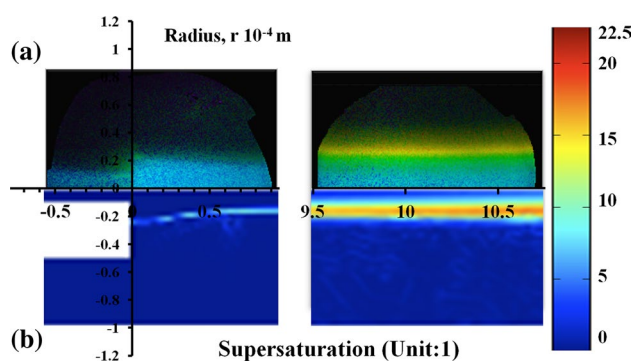


**Fig. 11** Comparison of real experimental FLIM imaging in (a) with the 2D-axisymmetric geometry of the glass microfluidic device and COMSOL simulations of Adambodipy supersaturation profile under the same condition (b), initial concentration of 0.08 mM and with flow rate  $Q_c = 0.8 \mu\text{L min}^{-1}$ ,  $Q_s = 13.6 \mu\text{L min}^{-1}$  along the hydrodynamic focusing flow, same image as in Fig. 8. The simulated supersaturation variable is labeled with a rainbow color scale with unit 1 (color figure online)

precipitation. As a consequence, the fluorescence lifetime remains inside the focused stream for a long time as demonstrated in the FLIM image (Figs. 8, 9b). At the interface for  $10 \mu\text{m} < r < 12 \mu\text{m}$ , the high water concentration induces nucleation and shorter lifetime (Figs. 8, 9b, 11).

### 3.3 The further simulation

We see on the FLIM image that the first nucleation has already started at  $0.9 \text{ mm} \pm 50 \mu\text{m}$ . From the comparison of the simulation with the experiment, we can conclude that the supersaturation range required for nucleation is expressed as  $8 \lesssim \frac{C_{\text{Adambodipy}}}{C_{\text{eq}}} \lesssim 15$ . The simulation explains why under these mixing conditions we do not observe the formation of a crystalline tube at the tip of the capillary: The supersaturation is lower than that required for nucleation to occur.

The COMSOL simulation does not include the nucleation process. The molecules are allowed to diffuse, the supersaturation is calculated, but the precipitation process is not included. Thus, at the onset of the precipitation, the supersaturation is overestimated.

## 4 Conclusion

In summary, we have presented a three-dimensional hydrodynamic focusing microfluidic system to produce Adambodipy organic nanoparticles (NPs) and to control the precipitation process. The results demonstrate that the NPs of controlled size can be synthesized by varying the focusing ratios. With a higher focusing ratio ( $Q_s/Q_c$ ), smaller nanoparticles can be produced thanks to faster and more efficient mixing conditions.

FLIM monitoring of a microfluidic system can measure in situ the evolution of the dye in the focused flow. The mixing of the solvents inside the channel and the study of the crystallization process are followed from a few milliseconds to a second. The multi-exponential fluorescence decay and its evolution allow the distinction between monomers in solution, the emerging nanostructures and final NPs. Combined with the dynamic light scattering measurements, the size distribution of the NPs displays a dynamic width that depends on the focusing stream.

Using COMSOL, the kinetics of the diffusion controlled process occurring in the microfluidic device was analyzed numerically. The simulation predicts the species diffusion and supersaturation field and allows the quantification of the experimental precipitation process.

**Acknowledgments** The authors thank the EDSP (*École Doctorale Sciences Pratiques*) of ENS (*École Normale Supérieure*) of Cachan for funding the Ph.D. thesis of Y–Y.L.

## References

- Abraham FF (1974) Homogeneous nucleation theory. Academic Press, New York
- Baba K, Kasai H, Okada S, Oikawa H, Nakanishi H (2003) Fabrication of organic nanocrystals using microwave irradiation and their optical properties. *Opt Mater* 21(1–3):591–594. doi:10.1016/S0925-3467(02)00206-9
- Badre S, Monnier V, Meallet-Renault R, Dumas-Verdes C, Schmidt EY, Mikhaleva AI, Laurent G, Levi G, Ibanez A, Trofimov BA, Pansu RB (2006) Fluorescence of molecular micro and nanocrystals prepared with Bodipy derivatives. *J Photochem Photobiol A* 183(3):238–246. doi:10.1016/j.jphotochem.2006.07.002
- Boreham A, Kim TY, Spahn V, Stein C, Mundhenk L, Gruber AD, Haag R, Welker P, Licha K, Alexiev U (2011) Exploiting fluorescence lifetime plasticity in FLIM: target molecule localization in cells and tissues. *ACS Med Chem Lett* 2(10):724–728. doi:10.1021/ML200092m
- Calleja V, Ameer-Beg SM, Vojnovic B, Woscholski R, Downward J, Larijani B (2003) Monitoring conformational changes of proteins in cells by fluorescence lifetime imaging microscopy. *Biochem J* 372(1):33–40. doi:10.1042/BJ20030358
- Chung HR, Kwon E, Kawa H, Kasai H, Nakanishi H (2006) Effect of solvent on organic nanocrystal growth using the reprecipitation method. *J Cryst Growth* 294(2):459–463. doi:10.1016/j.jcrysgro.2006.07.010
- Darken LS (1948) Diffusion, mobility and their interrelation through free energy in binary metallic systems. *T Am I Min Met Eng* 175:184–201. doi:10.1007/s11661-010-0177-7
- Génot V, Desportes S, Croushore C, Lefèvre J-P, Pansu RB, Delaie JA, von Rohr PR (2010) Synthesis of organic nanoparticles in a 3D flow focusing microreactor. *Chem Eng J* 161(1–2):234–239. doi:10.1016/j.cej.2010.04.029
- Guevara-Carrion G, Nieto-Drachi C, Vrabec J, Hasse H (2008) Prediction of transport properties by molecular simulation: methanol and ethanol and their mixture. *J Phys Chem B* 112(51):16664–16674. doi:10.1021/jp805584d
- Harrison DJ, Fluri K, Seiler K, Fan ZH, Effenhauser CS, Manz A (1993) Micromachining a miniaturized capillary electrophoresis-based chemical-analysis system on a chip. *Science* 261(5123):895–897. doi:10.1126/science.261.5123.895

- Hessel V, Lowe H, Schonfeld F (2005) Micromixers—a review on passive and active mixing principles. *Chem Eng Sci* 60(8–9):2479–2501. doi:[10.1016/J.Ces.2004.11.033](https://doi.org/10.1016/J.Ces.2004.11.033)
- Hibara A, Nonaka M, Tokeshi M, Kitamori T (2003) Spectroscopic analysis of liquid/liquid interfaces in multiphase microflows. *J Am Chem Soc* 125(49):14954–14955. doi:[10.1021/ja0373081](https://doi.org/10.1021/ja0373081)
- Holz M, Heil SR, Sacco A (2000) Temperature-dependent self-diffusion coefficients of water and six selected molecular liquids for calibration in accurate H-1 NMR PFG measurements. *Phys Chem Chem Phys* 2(20):4740–4742. doi:[10.1039/B005319H](https://doi.org/10.1039/B005319H)
- Jouyban A, Acree WE (2006) In silico prediction of drug solubility in water–ethanol mixtures using Jouyban–Acree model. *J Pharm Pharm Sci* 9(2):262–269. doi:[10.1691/ph.2007.1.6057](https://doi.org/10.1691/ph.2007.1.6057)
- Kakuta M, Hinsmann P, Manz A, Lendl B (2003a) Time-resolved Fourier transform infrared spectrometry using a microfabricated continuous flow mixer: application to protein conformation study using the example of ubiquitin. *Lab Chip* 3(2):82–85. doi:[10.1039/B302295a](https://doi.org/10.1039/B302295a)
- Kakuta M, Jayawickrama DA, Wolters AM, Manz A, Sweedler JV (2003b) Micromixer-based time-resolved NMR: applications to ubiquitin protein conformation. *Anal Chem* 75(4):956–960. doi:[10.1021/ac026076q](https://doi.org/10.1021/ac026076q)
- Kamholz AE, Schilling EA, Yager P (2001) Optical measurement of transverse molecular diffusion in a microchannel. *Biophys J* 80(4):1967–1972. doi:[10.1016/S0006-3495\(01\)76166-8](https://doi.org/10.1016/S0006-3495(01)76166-8)
- Khattab IS, Bandarkar F, Fakhree MAA, Jouyban A (2012) Density, viscosity, and surface tension of water plus ethanol mixtures from 293 to 323 K. *Korean J Chem Eng* 29(6):812–817. doi:[10.1007/s10953-014-0257-1](https://doi.org/10.1007/s10953-014-0257-1)
- Knight JB, Vishwanath A, Brody JP, Austin RH (1998) Hydrodynamic focusing on a silicon chip: mixing nanoliters in microseconds. *Phys Rev Lett* 80(17):3863–3866. doi:[10.1103/PhysRevLett.80.3863](https://doi.org/10.1103/PhysRevLett.80.3863)
- Kuhn HFH-D, Waldeck DH (2009) Principles of physical chemistry, vol 14. Wiley, Hoboken
- Li XY, Liu HJ, Sun XX, Bi GQ, Zhang GQ (2013) Highly fluorescent dye-aggregate-enhanced energy-transfer nanoparticles for neuronal cell imaging. *Adv Opt Mater* 1(8):549–553. doi:[10.1002/adom.201300173](https://doi.org/10.1002/adom.201300173)
- Liao Y-Y, Génot V, Meallet-Renault R, Vu TT, Audibert JF, Lemaitre JP, Clavier G, Retailleau P, Pansu RB (2013) Spectroscopy of BODIPY in solid phase: crystal and nanoparticles. *Phys Chem Chem Phys* 15(9):3186–3195. doi:[10.1039/c2cp43289g](https://doi.org/10.1039/c2cp43289g)
- Lin HJ, Herman P, Lakowicz JR (2003) Fluorescence lifetime-resolved pH imaging of living cells. *Cytometry A* 52(2):77–89. doi:[10.1002/cyto.a.10028](https://doi.org/10.1002/cyto.a.10028)
- Meallet-Renault R, Herault A, Vachon JJ, Pansu RB, Amigoni-Gerbier S, Larpent C (2006) Fluorescent nanoparticles as selective Cu(II) sensors. *Photochem Photobiol Sci* 5(3):300–310. doi:[10.1039/B513215K](https://doi.org/10.1039/B513215K)
- Nielsen AE (1964) Kinetics of precipitation. Pergamon Press, New York
- Ofuji M, Lovinger AJ, Kloc C, Siegrist T, Maliakal AJ, Katz HE (2005) Organic semiconductor designed for lamination transfer between polymer films. *Chem Mater* 17(23):5748–5753. doi:[10.1021/Cm0516w](https://doi.org/10.1021/Cm0516w)
- Roth CM, Heinlein PI, Heilemann M, Herten DP (2007) Imaging diffusion in living cells using time-correlated single-photon counting. *Anal Chem* 79(19):7340–7345. doi:[10.1021/Ac071039q](https://doi.org/10.1021/Ac071039q)
- Spitz JA, Yasukuni R, Sandeau N, Takano M, Vachon JJ, Meallet-Renault R, Pansu RB (2008) Scanning-less wide-field single-photon counting device for fluorescence intensity, lifetime and time-resolved anisotropy imaging microscopy. *J Microsc-Oxford* 229(1):104–114. doi:[10.1111/j.1365-2818.2007.01873.x](https://doi.org/10.1111/j.1365-2818.2007.01873.x)
- Su YF, Kim H, Kovenklioglu S, Lee WY (2007) Continuous nanoparticle production by microfluidic-based emulsion, mixing and crystallization. *J Solid State Chem* 180(9):2625–2629. doi:[10.1016/j.jssc.2007.06.033](https://doi.org/10.1016/j.jssc.2007.06.033)
- Teixeira R, Andrade SM, Serra VV, Paulo PMR, Sanchez-Coronilla A, Neves MGPMS, Cavaleiro JAS, Costa SMB (2012) Reorganization of self-assembled dipeptide porphyrin J-aggregates in water–ethanol mixtures. *J Phys Chem B* 116(8):2396–2404. doi:[10.1021/jp2115719](https://doi.org/10.1021/jp2115719)